CHIN. PHYS. LETT. Vol. 33, No. 3 (2016) 037303

Spin Caloritronic Transport of 1,3,5-Triphenylverdazyl Radical *

Qiu-Hua Wu(吴秋华)[1], Peng Zhao(赵朋)[1**], De-Sheng Liu(刘德胜)[2]

[1]*School of Physics and Technology, University of Jinan, Jinan 250022*

[2]*School of Physics, Shandong University, Jinan 250100*

(Received 9 October 2015)

We investigate theoretically the spin caloritronic transport properties of a stable 1,3,5-triphenylverdazyl (TPV) radical sandwiched between Au electrodes through different connection fashions. Obvious spin Seebeck effect can be observed in the para-connection fashion. Furthermore, a pure spin current and a completely spin-polarized current can be realized by tuning the gate voltage. Furthermore, a 100% spin polarization without the need of gate voltage can be obtained in the meta-connection fashion. These results demonstrate that TPV radical is a promising material for spin caloritronic and spintronic applications.

PACS: 73.23.−b, 85.65.+h, 71.15.Mb DOI: 10.1088/0256-307X/33/3/037303

As silicon-based technology approaches its limits, molecular electronics is becoming a burgeoning field that offers new miniaturization strategies in electronic devices.[1] However, dissipated heat becomes increasingly severe as the dimensions of devices become smaller and smaller. This not only brings about high energy consumption, but also reduces the reliability of devices. One promising solution relies on thermoelectric materials (the study of them is called thermoelectronics), a class of materials that can convert heat energy directly into electrical energy.[2,3] Moreover, spintronics, which seeks to exploit the spin degree of freedom of an electron in addition to its charge, provides a hopeful way to reduce the dissipated heat due to the small spin interactions.[4,5] Thus spin caloritronics, the combination of thermoelectronics and spintronics, have attracted considerable attention.[6,7] A landmark in this field is the recent observation of the spin Seebeck effect (SSE).[8] In SSE, the spin-up current and spin-down current, flowing in opposite directions, can be induced by a temperature difference rather than by a bias voltage. The spin-polarized currents can be further converted to spin voltages by the inverse spin Hall effect.[9−11] Then the dissipated heat energy is transformed into the spin-polarized current/voltage to be re-utilized.

Organic radicals, composed of light elements such as C, N, O, S and H, can exhibit magnetism due to their unpaired electrons. They have recently been considered as suitable candidates with long spin coherent length for spintronics due to the fact that light elements in them have small spin-orbital coupling and hyperfine interactions.[12−15] Among them, 1,3,5-triphenylverdazyl (TPV) is an unusually stable one, which has a spin doublet ground state.[16] The unpaired electron in TPV delocalizes over all four N atoms. Owing to the delocalization, TPV is so stable that it can be stored for years safely just like closed-shell organic compounds.[17−19] In this work, we investigate for the first time the spin caloritronic transport properties of the TPV radical linked to the Au electrodes through different connection methods.

The devices under study are depicted in Figs. 1(a) and 1(b), the TPV is bonded to the Au(111) electrodes via the S atom through para- or meta-connection, respectively. A gate voltage V_g is adopted to tune the transport properties.[20,21] An external magnetic field ($\otimes$) is applied to keep the magnetism of TPV radical at high temperatures.[22] Initially, the S atom is located at 1.71 Å from the hollow site of Au(111) surface.[23−25] Such devices can be partitioned into three regions: a source/drain electrode (SE/DE) and a central scattering region (CSR). In addition to the TPV, three Au layers from each electrode are also included into the CSR to screen the potential effect of TPV on the electrodes. The geometries of these devices are relaxed with a convergence force criterion of 0.05 eV/Å.

Structural optimizations and calculations of transport properties are carried out by using the ATK software,[26,27] which combines nonequilibrium Green's function (NEGF) with density functional theory (DFT). Due to the long spin diffusion length and weak electron–phonon coupling in organic radicals,[12−15] the coherent transport mechanism is assumed in our work. Exchange correlation is taken into account within the spin-polarized generalized gradient approximation with the Perdew–Burke–Ernzerhof functional.[28] The norm-conserving Troullier–Martins pseudopotentials[29] are employed to model the core electrons of all atoms. The single-zeta plus polarization basis set for the valence elec-

*Supported by the National Natural Science Foundation of China under Grant No 11104115, and the Science Foundation of Middle-aged and Young Scientist of Shandong Province of China under Grant No BS2013DX036.

**Corresponding author. Email: ss_zhaop@ujn.edu.cn

© 2016 Chinese Physical Society and IOP Publishing Ltd

trons of Au atoms and the double-zeta plus polarization basis set for the valence electrons of all the other atoms are used. A plane-wave cutoff is set to 150 Ry. A $3 \times 3 \times 100$ k-mesh is used to sample the Brillouin zone of SE/DE. The thermal spin-polarized current is calculated by the Landauer–Büttiker formula,[30] $I_\sigma = (e/h)\int_{-\infty}^{\infty} T_\sigma(E)[f_S(E,T_S) - f_D(E,T_D)]dE$, where σ is the spin index, σ=up/dn (spin-up/spin-down), T_σ is the transmission function, $f_{S/D}$ is the Fermi–Dirac distribution function, and $T_{S/D}$ is the temperature of SE/RE, respectively.

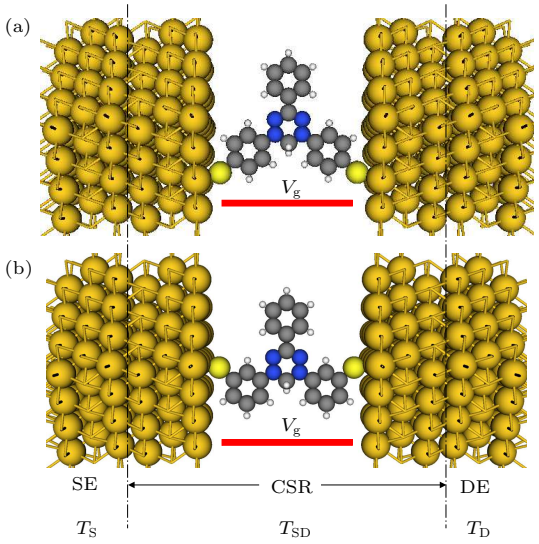

Fig. 1. TPV radical sandwiched between the Au electrodes via the S atom through (a) para- and (b) meta-connection methods. The spin-polarized currents can be generated by a temperature difference (T_{SD}) between the source electrode (SD) and the drain electrode (DE). The central scattering region (CSR) includes the TPV and three Au layers from each electrode. A gate voltage (V_g) is adopted to tune the thermally induced spin-polarized currents. An external magnetic field ($\otimes$) is applied to keep the magnetism of TPV at high temperatures. Atomic species are shown in gold for Au, yellow for S, gray for C, blue for N, and white for H, respectively.

As shown in Figs. 1(a) and 1(b), the spin-polarized currents are caused by a temperature difference (T_{SD}) between the source and drain electrode, i.e., $T_{SD} = T_S - T_D$, without the external bias voltage. We first investigate the para-connection fashion. Figure 2(a) plots the spin-polarized currents versus T_{SD}, where T_S varies from 100 to 300 K. Clearly, the spin-up currents (I_{up}) are positive and the spin-down currents (I_{dn}) are negative, which is an obvious SSE. Moreover, the magnitude of I_{up} is significantly larger than that of I_{dn}. Both of them increase almost linearly with T_{SD} or T_S. The spin polarization, SP=$[(|I_{up}|-|I_{dn}|)/(|I_{up}|+|I_{dn}|)]\times 100\%$, versus T_{SD} for different T_S is presented in Fig. 2(b). Clearly, the SP keeps nearly constant with the increase of T_{SD} when T_S is fixed since I_{up}/I_{dn} is almost proportional to T_{SD}. However, it decreases gradually from ~86% with $T_S = 100$ K, to ~82% with $T_S = 200$ K, and to ~72% with $T_S = 300$ K.

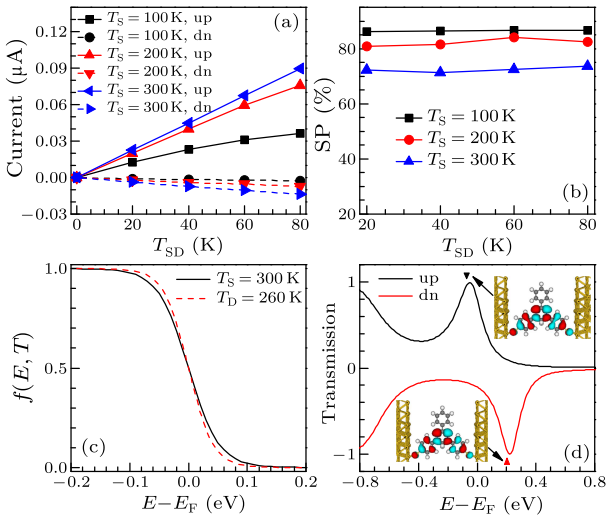

Fig. 2. (a) The spin-polarized currents versus T_{SD} for the para-connection fashion, where T_S varies from 100 to 300 K. (b) The spin polarization (SP) versus T_{SD} for different T_S. (c) The Fermi–Dirac distribution of SE/RE with $T_S = 300$ K/$T_D = 260$ K. (d) The transmission spectra with $T_S = T_D = 300$ K, which keep nearly unchanged within the considered T_{SD} range. The positions of HOMO and LUMO are marked with black down-triangle and red up-triangle, respectively. The insets show the spatial distribution of HOMO and LUMO, and the different colors indicate the phase of wavefunctions.

According to the Landauer–Büttiker formula, the spin-polarized currents are caused by the combined effects of T_σ and $(f_S - f_D)$. Figure 2(c) plots f_S with $T_S = 300$ K and f_D with $T_D = 260$ K versus the carrier energy (E), where the Fermi level (E_F) is set to 0 eV. As one can see, $f_S < f_D$ when $E < E_F$, the carriers (holes) flow from the SE to the DE, leading to a positive current. On the other hand, $f_S > f_D$ when $E > E_F$, the carriers (electrons) also flow from the SE to the DE, resulting in a negative current in the opposite direction. Moreover, both f_S and f_D are symmetric with respect to E_F. Then, $(f_S - f_D)$ is symmetric about E_F. Therefore, if T_σ is also symmetric with respect to E_F, the currents induced by the holes and electrons will cancel out each other, resulting in a zero net current. This indicates that an asymmetric distribution of T_σ around E_F is a prerequisite to obtain a nonzero current. Figure 2(d) plots T_σ, in which both the spin-up and spin-down transmission spectra (T_{up} and T_{dn}) around E_F display obvious asymmetric features, that is, a broad spin-up/spin-down peak locates around $-0.07/0.20$ eV, which originates from the highest occupied molecular orbital (HOMO)/lowest unoccupied molecular orbital (LUMO). As shown in Fig. 2(d), the positions of HOMO and LUMO are marked with black down-triangle and red up-triangle, respectively. Evidently, they correspond nicely with the transmission peaks. Here we must point out that these two molecular orbitals are calculated from the molecular projected self-consistent Hamiltonian (MPSH), i.e., the

self-consistent Hamiltonian of the central molecule in the presence of electrodes.[31] As shown in the insets of Fig. 2(d), both HOMO and LUMO are delocalized orbitals, leading to the two broad transmission peaks around E_F.

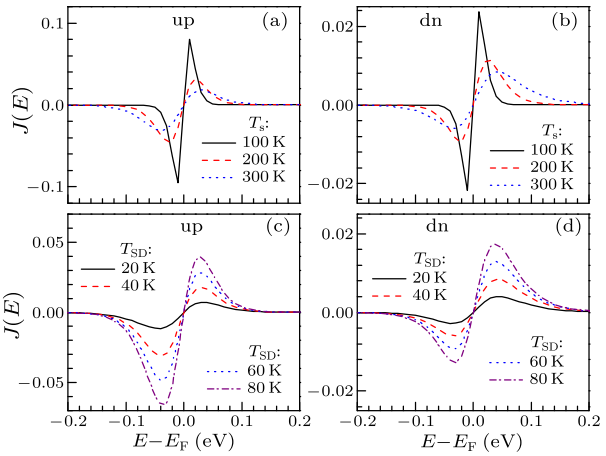

Fig. 3. The spin-up (a) and spin-down (b) current spectra for different T_S with $T_{SD} = 40$ K, and the spin-up (c) and spin-down (d) current spectra for different T_{SD} with $T_S = 300$ K.

To further elucidate the combined effects of T_σ and $(f_S - f_D)$ on the currents, in Fig. 3 we present the current spectra $J_\sigma(E) = T_\sigma(E)[f_S(E,T_S) - f_D(E,T_D)]$. Figures 3(a) and 3(b) correspond to the spin-up and spin-down current spectra (J_{up} and J_{dn}) for different T_S with $T_{SD} = 40$ K. Figures 3(c) and 3(d) correspond to J_{up} and J_{dn} for different T_{SD} with $T_S = 300$ K. All current spectra display a typical exponential decaying nature and an asymmetric feature around E_F. As shown in Fig. 3(a) (Fig. 3(b)), when T_{SD} is fixed, at $T_S = 100$ K, the peak of J_{up} (J_{dn}) below E_F is slightly higher (lower) than that above E_F, leading to a small positive (negative) net I_{up} (I_{dn}). When T_S goes up further, the peaks of the current spectrum below and above E_F become lower and wider. However, the difference between the cover area of J_{up} (J_{dn}) below (above) E_F and the one above (below) E_F increases gradually, resulting in the enhancement of I_{up} (I_{dn}) with the increase of T_S. As shown in Fig. 3(c) (Fig. 3(d)), when T_S is fixed, the peaks of current spectrum below and above E_F become higher and higher with the increase of T_{SD}, and the difference between the cover area of J_{up} (J_{dn}) below (above) E_F and the one above (below) E_F increases gradually. Therefore, both I_{up} and I_{dn} go up with the increase of T_{SD} accordingly. Moreover, the difference between the cover area of J_{up} below E_F and the one above E_F is always larger than that of J_{dn}. As a result, I_{up} is always larger than I_{dn} at the same T_S and T_{SD}.

Since the currents are strongly dependent on the transmission peaks around E_F, which can be modulated effectively by applying a V_g,[20,21] in Fig. 4(a), we plot I_{up} and I_{dn} versus V_g with $T_S = 300$ K and $T_{SD} = 40$ K. Evidently, the magnitude of I_{up} decreases rapidly with the increase of V_g. At $V_g = 0.6$ V, $I_{up} = 0$. When V_g goes up further, I_{up} changes its sign from positive to negative and its magnitude increases quickly again. By contrast, I_{dn} is always negative within the considered V_g range, and its magnitude increases slowly with the increase of V_g. The inset of Fig. 4(a) plots SP versus V_g. Clearly, SP can be tuned effectively, especially at $V_g = 0.6$ V, SP reaches -100% due to $I_{up} = 0$ and $I_{dn} \neq 0$. This indicates that it is possible to obtain a 100% spin-polarized current by applying an appropriate V_g. In Fig. 4(b), we further plot the total charge current I_C and total spin current I_S, defined as $I_C = I_{up} + I_{dn}$ and $I_S = I_{up} - I_{dn}$, versus V_g, respectively. Interestingly, I_C vanishes completely at $V_g = 0.52$ V, where $I_S \neq 0$, therefore, we can achieve a pure spin current by tuning V_g, which has important applications in spintronics.[32]

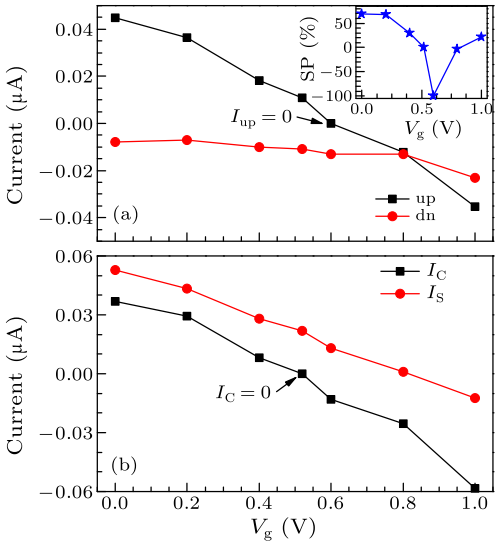

Fig. 4. (a) The spin-polarized currents versus V_g with $T_S = 300$ K and $T_{SD} = 40$ K. The inset shows the SP versus V_g. At $V_g = 0.6$ V, the SP reaches -100% due to $I_{up} = 0$ and $I_{dn} \neq 0$. (b) The total charge current I_C ($I_C = I_{up} + I_{dn}$) and the total spin current I_S ($I_S = I_{up} - I_{dn}$) versus V_g. A pure spin current appears at $V_g = 0.52$ V, where $I_C = 0$ and $I_S \neq 0$.

Finally, we investigate the meta-connection fashion. Figure 5(a) plots the calculated T_σ. Similar to the para-connection one, there is also an HOMO-derived spin-up peak around -0.07 eV, which can give rise to an obvious I_{up}. However, the LUMO-derived spin-down peak is around 0.50 eV, which is too far away from E_F to contribute I_{dn} due to the typical exponential decaying nature of current spectra. Moreover, the transmission peaks of meta-connection fashion are strongly narrowed compared with those of para-connection fashion, which can be ascribed to the destructive interference in the meta-connection fashion.[13,33] This point can be further understood by the spatial distributions of HOMO and LUMO, as

shown in the insets of Fig. 5(a), both of them are localized orbitals, which cause weak molecule–electrode couplings and narrowed transmission peaks. Figure 5(b) presents the corresponding spin-polarized currents versus $T_{\rm SD}$. Clearly, $I_{\rm up}$ increases rapidly with $T_{\rm SD}$, while $I_{\rm dn}$ is strongly blocked. As a result, a 100% spin polarization is achieved without the need of $V_{\rm g}$.

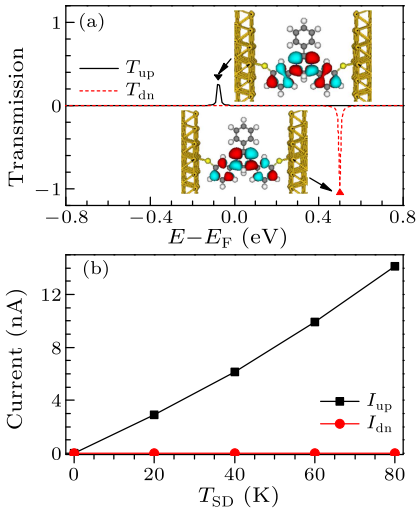

Fig. 5. (a) The transmission spectra for the meta-connection fashion with $T_{\rm S} = T_{\rm D} = 300\,{\rm K}$. The positions of HOMO and LUMO are marked with black down-triangle and red up-triangle. The insets show the spatial distributions of HOMO and LUMO. (b) The corresponding spin-polarized currents versus $T_{\rm SD}$ with $T_{\rm S} = 300\,{\rm K}$.

In conclusion, we have proposed the TPV radical-based spin caloritronic devices, in which the TPV is sandwiched between two Au electrodes through para- or meta-connection fashions. By using the DFT+NEGF approach, the spin caloritronic transport properties have been investigated. Obviously SSE can be generated in the para-connection fashion due to the asymmetry of both $T_{\rm up}$ and $T_{\rm dn}$ with respect to $E_{\rm F}$. Furthermore, the thermally induced spin-polarized currents can be effectively tuned by $V_{\rm g}$, which in turn can be utilized to create a pure spin current and a completely spin-polarized current. Moreover, in the meta-connection fashion, the spin-down current is found to be entirely blocked, resulting in a 100% spin polarization without the need of $V_{\rm g}$. These results demonstrate that the TPV radical is a promising material for spin caloritronic and spintronic applications.

References

[1] Joachim C, Gimzewski J K and Aviram A 2000 *Nature* **408** 541
[2] Zebarjadi M, Esfarjani K, Dresselhaus M S, Ren Z F and Chen G 2012 *Energy Environ. Sci.* **5** 5147
[3] Poehler T O and Katz H E 2012 *Energy Environ. Sci.* **5** 8110
[4] Wolf S, Awschalom D, Buhrman R, Daughton J, von Molnar S, Roukes M, Chtchelkanova A and Treger D 2001 *Science* **294** 1488
[5] Fert A 2008 *Rev. Mod. Phys.* **80** 1517
[6] Bauer G E W, Saitoh E and van Wees B J 2012 *Nat. Mater.* **11** 391
[7] Boona S R, Myers R C and Heremans J P 2014 *Energy Environ. Sci.* **7** 885
[8] Uchida K, Takahashi S, Harii K, Ieda J, Koshibae W, Ando K, Maekawa S and Saitoh E 2008 *Nature* **455** 778
[9] Valenzuela S and Tinkham M 2006 *Nature* **442** 176
[10] Saitoh E, Ueda M, Miyajima H and Tatara G 2006 *Appl. Phys. Lett.* **88** 182509
[11] Kimura K, Otani Y, Sato T, Takahashi S and Maekawa S 2007 *Phys. Rev. Lett.* **98** 156601
[12] Rajca A 1994 *Chem. Rev.* **94** 871
[13] Herrmann C, Solomon G C and Ratner M A 2010 *J. Am. Chem. Soc.* **132** 3682
[14] Matsuura Y 2015 *Chem. Phys. Lett.* **619** 23
[15] Rocha A R, Garcia-Suarez V M, Bailey S W, Lambert C J, Ferrer J and Sanvito S 2005 *Nat. Mater.* **4** 335
[16] Kuhn R and Trischmann H 1963 *Angew. Chem. Int. Ed.* **2** 155
[17] Kuhn R and Trischmann H 1964 *Monatsh. Chem.* **95** 457
[18] Azuma N, Yamauchi J, Mukai K, Ohya-Nishiguchi H and Deguchi Y 1973 *Bull. Chem. Soc. Jpn.* **46** 2728
[19] Allemand P M, Srdanov G and Wudl F 1990 *J. Am. Chem. Soc.* **112** 9391
[20] Zhao P, Liu D S, Liu H Y, Li S J and Chen G 2013 *Org. Electron.* **14** 1109
[21] Wu Q H, Zhao P and Liu D S 2014 *Phys. Lett.* A **378** 561
[22] Kim W Y and Kim K S 2008 *Nat. Nanotechnol.* **3** 408
[23] Larsen N, Biebuyck H, Delamarche E and Michel B 1997 *J. Am. Chem. Soc.* **119** 3017
[24] Damle P, Rakshit T, Paulsson M and Datta S 2002 *IEEE Trans. Nanotechnol.* **1** 145
[25] Andreoni W, Curioni A and GrönbeckH 2000 *Int. J. Quantum Chem.* **80** 598
[26] Taylor J, Guo H and Wang J 2001 *Phys. Rev.* B **63** 245407(R)
[27] Brandbyge M, Mozos J L, Ordejón P, Taylor J and Stokbro K 2002 *Phys. Rev.* B **65** 165401
[28] Perdew J P, Burke K and Ernzerhof M 1996 *Phys. Rev. Lett.* **77** 3865
[29] Troullier N and Martins J 1991 *Phys. Rev.* B **43** 1993
[30] Büttiker M, Imry Y, Landauer R and Pinhas S 1985 *Phys. Rev.* B **31** 6207
[31] Stokbro K, Taylor J, Brandbyge M, Mozos J L and Ordejón P 2003 *Comput. Mater. Sci.* **27** 151
[32] Chappert C, Fert A and van Dau F N 2007 *Nat. Mater.* **6** 813
[33] Ke S H, Yang W and Baranger H U 2008 *Nano Lett.* **8** 3257